NASA TM-84334

NASA-TM-84334 19830021365

Numerical Simulation of Vortex Breakdown by the Vortex-Filament Method

Y. Nakamura, A. Leonard, and P.R. Spalart

July 1983

NASA
National Aeronautics and
Space Administration

Numerical Simulation of Vortex Breakdown by the Vortex-Filament Method

Y. Nakamura,
A. Leonard,
P. R. Spalart, Ames Research Center, Moffett Field, California

NUMERICAL SIMULATION OF VORTEX BREAKDOWN BY THE VORTEX-FILAMENT METHOD

Y. Nakamura, A. Leonard, and P. R. Spalart
NASA Ames Research Center, Moffett Field, California 94035, U.S.A.

SUMMARY

The vortex-filament method was applied to the simulation of vortex breakdown. The principal vortex region was represented by multiple filaments, and an axial velocity component was induced by a spiral winding of the filaments. First, an accuracy check was performed for a cylindrical swirling flow with simple analytical expressions for the axial and theta velocities. The result suggests that the flow field can be simulated to any accuracy by increasing the number of filaments. Second, an axisymmetric-type vortex breakdown was simulated, with experimental data serving as upstream conditions. The calculated axial- and theta-velocity contours show the breakdown of the vortex, including a rapid change in the vortex core, followed axially by a recovery zone and then a second breakdown. When three-dimensional initial data are used the second breakdown appears to be of the spiral type in correspondence with experimental observations. The present method can easily be used to simulate other types of vortex breakdown or other vortex flows with axial velocity.

1. INTRODUCTION

The phenomenon of vortex breakdown is not only of fundamental interest, but is of considerable importance in aerodynamics as well. For example, vortex breakdown over a wing usually affects the aerodynamic performance of that wing. In fact, one of the first experimental studies of vortex breakdown was Peckham and Atkinson's investigation (Ref. 1) of flow over a delta wing. At high incidence they observed breakdown (usually defined as an abrupt change along the vortex axis with a limited region of flow reversal) of the pair of vortices formed at the leading edge of a delta wing. Since then many other experiments of vortex breakdown have been carried out. Those studies revealed three basic patterns of breakdown: axisymmetric, spiral, and double-helix. Flow visualizations by Sarpkaya (Ref. 2) show these patterns in water. He systematically measured the relationship between Reynolds number, the position of breakdown, the pattern of breakdown, and the amount of swirling. Lambourne and Bryer's study of flow over a delta wing (Ref. 3; see also Ref. 4) clearly shows two different patterns of vortex breakdown, axisymmetric and spiral, occurring at the same time. Recently, Faler and Leibovich proposed a more detailed classification scheme for vortex breakdown based on extensive observations (Ref. 5) and obtained measurements of velocity profiles using a laser Doppler velocimeter (Ref. 6). Escudier and Zehnder (Ref. 7) have proposed a simple criterion for vortex breakdown, using extensive flow-visualization data. See Hall (Ref. 4) and Leibovich (Ref. 8) for a review of these studies, as well as theoretical efforts on vortex breakdown.

On the theoretical side, Benjamin's finite transition theory (Ref. 9) proposes that the breakdown of swirling flow corresponds to the transition from supercritical to subcritical flow in a hydraulic jump in open-channel flow. On the other hand, Ludwieg (Ref. 10) proposed an instability theory for swirling flows in which vortex breakdown is attributed to the growth of instability waves on the vortex core by increasing helical interference vortices.

In an attempt to treat vortex breakdown numerically, Hall (Ref. 11) derived a boundary-layer-like equation and solved it by a marching method. This scheme assumes axisymmetric, steady flow and can treat an arbitrary upstream flow field. Since the equation itself is parabolic, there is some dispute over whether this type of equation is valid for sudden changes in flow structure. More recently, Grabowski and Berger (Ref. 12) solved the Navier-Stokes equations, using Chorin's artificial compressibility method, to simulate axisymmetric vortex breakdown. This scheme also assumes steady flow and appears to be limited to low Reynolds numbers.

It is clearly desirable to attack the vortex-breakdown problem numerically with a three-dimensional capability. According to detailed observations, even an axisymmetric-type vortex breakdown includes three-dimensional motion. In this paper, we present the result of numerical simulations of vortex breakdown, using the three-dimensional vortex-filament method developed by Leonard (Ref. 13). In particular, we have studied the axisymmetric breakdown. Our present results are for both axisymmetric and three-dimensional initial data. It is our view that the primary role of Reynolds number is in shaping the internal structure of the vortex core upstream of the breakdown. As shown below, the upstream conditions can be duplicated by proper choice of the filament geometry and strength. The process of breakdown occurs rapidly and is therefore dominated by nonlinear inviscid phenomena, well described by the dynamics of the vortex-filament method. In a similar approach, Del Prete (Ref. 14) modeled vortex breakdown using the vortex method. However, she used only parallel longitudinal vortex filaments upstream — with no axial velocity component — interacting with a vortex ring to produce a structure suggestive of vortex breakdown.

Although this report is concerned with the simulation of vortex breakdown, the method used can treat any system of vortices with or without axial velocity distribution and, for example, should be capable of simulating in detail the merging process of aircraft wake vortices.

2. NUMERICAL METHOD

The vortex-filament method was developed by Leonard (Ref. 13) and successfully applied to the wake-vortex interaction problem behind large jet aircraft (e.g., B-747) and to the spot-like disturbance in a laminar boundary layer. This method seems well suited to the simulation of vortex breakdown, in that computational elements are required only for the vorticity-containing fluid in and near the flow region where vortex breakdown is occurring. Furthermore, in the vortex filament method rapid changes in the flow pattern with three-dimensionality can be represented with minimal error due to numerical diffusion. The vortex-filament method is generalized from the two-dimensional vortex-blob method to three dimensions by assuming that the vorticity field is represented by a collection of tubes or filaments of vorticity defined

by the space curves $[\mathbf{r}_i(\xi,t), i = 1, 2, \ldots, L]$, where ξ is a parameter along the curve and L is the number of the vortex filaments. The vortex-filament method does not have a singular vorticity distribution inside the vortex filament as does the classical point-vortex method.

The dynamics of these filaments, consistent with the theorems of Helmholtz and Kelvin, is given by

$$\frac{\partial \mathbf{r}_i(\xi,t)}{\partial t} = -\frac{1}{4\pi} \sum_{j=1}^{L} \Gamma_j \int \frac{(\mathbf{r}_i - \mathbf{r}_j) \times (\partial \mathbf{r}_j/\partial\xi') s(|\mathbf{r}_i - \mathbf{r}_j|,\sigma_i,\sigma_j) d\xi'}{|\mathbf{r}_i - \mathbf{r}_j|^3} \tag{1}$$

The "s" function included in this equation is related to the vorticity distribution inside a vortex filament. Leonard (Ref. 13) gave two particular choices of the function "s." In this paper we use the so-called "scheme C," which is of the form

$$s(y,\sigma_i,\sigma_j) = \frac{1}{[1 + \alpha(\sigma_i^2 + \sigma_j^2)/2y^2]^{3/2}} \tag{2}$$

where the choice $\alpha = 0.413$ for a Gaussian distribution of vorticity within the core yields the correct speed of a single vortex ring.

In vortex-flow simulations, the following two flow representations are possible:

1. Single filament to represent each physical vortex

2. Multiple filaments to represent each physical vortex

The first method was used for test problems which are not described here. These are the interaction of four vortex rings and the interaction of two pairs of wake vortices that cross at a right angle with some clearance. The results were successful and convincing. In particular, the first case produced results very close to those of experiment (Ref. 15). These preliminary results were encouraging for the application of this method to vortex breakdown. However, the single-filament representation is appropriate only when the internal structure is not of major importance. The multiple-filaments representation has to be considered when the internal structure, including axial flow, has a significant effect on the dynamics. In this paper we use the latter representation to simulate vortex breakdown. If this method proves successful and if a detailed procedure is established, many new applications to practical flows dominated by vortices may be attempted.

3. ACCURACY CHECK OF THE VORTEX-FILAMENT METHOD

We first performed an accuracy check for the three-dimensional vortex-filament method. A flow with a simple analytical expression was chosen, and its vorticity was represented by vortex filaments. Then the velocity field induced by the filaments was compared with the idealized field. This method has two numerical parameters: the core radius and the initial spacing between the vortex filaments. The accuracy is expected to improve when the number of the filaments used is increased, which makes the average distance between neighboring vortex filaments smaller. It is also interesting to estimate the relation between the optimum core radius and the average distance. We did a similar study in two dimensions, with Gaussian cores (see Ref. 16). The results suggested the relation $\sigma \sim \delta^{0.875}$, where σ is the core radius and δ is the average distance. This means that the core radius should tend to zero more slowly than the average distance does.

For the test, it is convenient to choose a flow in which the vorticity sharply declines with the distance from the axis. The following expressions, often used for unbounded swirling flow, satisfy these requirements:

$$V_x = a_1 + a_2 \exp(-a_3 r^2) \tag{3}$$

$$V_\theta = \Gamma_0[1 - \exp(-b_1 r^2)]/r \tag{4}$$

$$V_r = 0 \tag{5}$$

where V_x is the axial-velocity component, V_θ the theta velocity, and V_r the radial velocity. The values actually used for the parameters are

$$a_1 = 0.95 , \quad a_2 = 1.55 , \quad a_3 = 10 , \quad b_1 = 10.9 , \quad \text{and} \quad \Gamma_0 = 0.825$$

which approximate those obtained in an experiment inside a pipe (private communication, Uchida et al., Nagoya Univ.), as shown in Fig. 1. We are not concerned with the wall region where, of course, the idealized velocity does not match the experimental velocity because we are simulating an unbounded flow. The measurements were obtained by a laser Doppler velocimeter for axisymmetric vortex breakdown at a Reynolds number of 2300. Figure 1a shows the axial velocity component of Eq. (3) which is high near the axis and approaches 0.95 (potential flow) as the radius increases. Needless to say, this profile includes the axial flow inside the vortex. Figure 1b shows the theta velocity, with almost rigid rotation near the axis and a maximum value at $r = 0.34$. Beyond this point the profile becomes proportional to $1/r$ and represents a potential swirling flow for larger values of the radius. Figure 2 shows the theta-vorticity distribution, which was calculated from the axial velocity by the relation $\omega_\theta = -dV_x/dr$, assuming a cylindrical flow. At $r = 0.22$, the theta vorticity has a maximum value. Figure 3 shows the axial-vorticity distribution, which was calculated from the theta velocity by the relation $\omega_x = d(rV_\theta)/dr/r$, assuming a cylindrical flow. This is a Gaussian distribution. Figure 4 shows the distribution of the circulation, which is calculated by the expression

2

$$\Gamma = 2\pi r V_\theta \qquad (6)$$

This has a familiar pattern of positive curvature near the x-axis approaching a constant value at infinity. Figure 5 shows the magnitude of the vorticity vector as a function of r. The deflection angle of the vorticity from the x-axis is also shown (dashed line); it increases monotonically with radius. Figure 6 shows a three-dimensional picture of the vorticity vector along the radial direction. It can be seen that the vorticity maintains a moderate deflection angle for all radii.

We now discuss the problem of discretizing the idealized vorticity field with helical vortex filaments. The circulation and helicity of each filament as well as their distribution in space must be chosen to represent the idealized vorticity field as well as possible. We divided the circular cross section radially into a number of zones or rings. Each radial zone in turn contains a number of filaments distributed uniformly in the azimuthal direction. In the present simulation we used more filaments per unit area near $r = 0$ where the vorticity is maximum. Using a nonuniform radial distribution of filaments allowed us to obtain a more accurate representation of the idealized flow.

First, we discuss the method used to obtain the filament circulations. For simplicity of analysis, we assume infinite, straight vortex filaments with axes in the x-direction, distributed continuously along the circumference of each ring at the radii r_i. We have the following expression for the axial vorticity produced by one of these cylindrical shells of vorticity

$$\hat{\omega}_{x_i} = \Gamma_{x_i} \int_{-\infty}^{\infty} \int_0^{2\pi} \gamma r_i \, d\theta \, dx' \qquad (7)$$

where Γ_{x_i} is the circulation per unit circumference, and γ is the distribution function of vorticity inside a filament which is calculated from Eq. (2) as follows:

$$\gamma(y) = (ds/dy)/4\pi y^2 = (3\alpha\sigma^2/4\pi)[y^2 + \alpha\sigma^2]^{-5/2} \qquad (8)$$

Equation (7) with substitution of Eq. (8) may be integrated analytically to obtain

$$\hat{\omega}_{x_i} \equiv \Gamma_{x_i}\psi_i = \Gamma_{x_i} \frac{2\alpha\sigma_i^2 r_i (r_i^2 + r^2 + \alpha\sigma_i^2)}{\{[(r_i + r)^2 + \alpha\sigma_i^2][(r_i - r)^2 + \alpha\sigma_i^2]\}^{3/2}} \qquad (9)$$

We determine the optimum circulation distribution Γ_{x_i} for given axial vorticity distribution by minimizing the square error with the total circulation fixed. This leads to the following expression for the H function

$$H = \int_0^\infty \left(\omega_x - \sum_i^N \Gamma_{x_i}\psi_i\right)^2 dr + \lambda\left(\sum_i^N 2\pi r_i \Gamma_{x_i} - C\right) \qquad (10)$$

where C is the total circulation. Differentiating H with respect to the Γ_{x_i} and λ yields the following simultaneous equations for Γ_{x_i}:

$$\left.\begin{array}{l} 2\sum_i^N \int_0^\infty \psi_i(r)\psi_k(r)dr\Gamma_{x_i} + \lambda 2\pi r_k = 2\int_0^\infty \omega_x\psi_k(r)dr \ , \quad k = 1,2,\ldots,N \\[20pt] \sum_i^N 2\pi r_i \Gamma_{x_i} = C \end{array}\right\} \qquad (11)$$

Solving Eqs. (11), we obtain the optimum circulation distribution Γ_{x_i} for each ring. If N_i is the number of filaments placed in the ith ring then the circulation of each of these filaments is given by

$$\Gamma_j = 2\pi r_i \Gamma_{x_i}/N_i \qquad (12)$$

The next step is to determine the angle each helical filament makes with the x-axis, the deviation angle. For this purpose we assume that the theta component of vorticity is distributed continuously and uniformly along the x-direction with Γ_{θ_i} circulation per unit axial length for the ith ring. Again, using Eq. (8) we find that the ith ring of distributed theta vorticity contributes to the theta vorticity component as follows

$$\hat{\omega}_{\theta_i} = \Gamma_{\theta_i} \frac{4zr_i^2\alpha\sigma_i^2}{[(r_i^2 - r^2)^2 + 2\alpha\sigma_i^2(r_i^2 + r^2) + \alpha^2\sigma_i^4]^{3/2}} \qquad (13)$$

The same minimization procedure used above was used to determine the optimum Γ_{θ_i} except that total vorticity constraint is not imposed in this case. Finally the deviation angle from the x-axis of each filament in ring i was determined by

$$\tan \alpha_j = \Gamma_{\theta_i}/\Gamma_{x_i} \qquad (14)$$

3

By using the circulations and deviation angles for each ring, we calculated the induced velocity at a cross section using the following expressions:

$$V_x = -(1/4\pi) \sum_{j=1}^{L} \Gamma_j \int_{-\infty}^{\infty} a_j R_j [r \sin(a_j x' + \hat{\theta}_j) - R_j]/F \, dx' \Bigg\rbrace$$

$$V_y = \sum_{j=1}^{L} (V_y' \sin \hat{\theta}_j - V_z' \cos \hat{\theta}_j) \tag{15}$$

$$V_z = \sum_{j=1}^{L} (V_y' \cos \hat{\theta}_j + V_z' \sin \hat{\theta}_j)$$

where

$$F = [x'^2 - 2yR_j \cos(a_j x') - 2zR_j \sin(a_j x') + R_j^2 + \alpha\sigma_j^2 + r^2]^{3/2}$$

$$V_y' = -(1/4\pi)\Gamma_j \int_{-\infty}^{\infty} [z \sin \hat{\theta}_j - y \cos \hat{\theta}_j - R_j \sin(a_j x') + a_j R_j x' \cos(a_j x')]/F \, dx'$$

$$V_z' = -(1/4\pi)\Gamma_j \int_{-\infty}^{\infty} [-y \sin \hat{\theta}_j - z \cos \hat{\theta}_j + R_j \cos(a_j x') + a_j R_j x' \sin(a_j x')]/F \, dx'$$

$$p_j = 2\pi/\lambda_j , \qquad \hat{\theta}_j = \theta_j - \theta$$

(R_j, θ_j) and (r, θ) are the coordinates of the filament and the point where the induced velocity is required, respectively, and p_j is the filament pitch. These expressions are obtained by transforming the original expressions of the induced velocities, written in the Cartesian coordinates, using the relations representing the spiral shape of the filaments.

As our first test of our discretized vorticity field we calculated the distribution of the induced, unperturbed axial and theta velocity components of the upstream flow, which for the test extended over the entire x-axis. The actual integration was performed numerically from -10 to 10 using Simpson's rule with a spacing of 0.04 for x. Four rings were used radially with radii at 0.06, 0.18, 0.30, and 0.42 with 6, 6, 8, and 8 filaments in the respective rings. The core radius σ of each filament was 0.16. The results along the z-axis are depicted in Fig. 7 and show very good agreement. To check for uniformity in the azimuthal direction we obtained contour plots of the induced velocity field in a plane normal to the x-axis. These are shown in Fig. 8 along with corresponding contours of the idealized field. Generally we obtained a very good representation of the idealized field with a tendency to slightly underestimate idealized values.

4. SIMULATION OF VORTEX BREAKDOWN

For conditions upstream of vortex breakdown we assumed the idealized flow from above and therefore we used the filament parameters determined above. There might be some dispute over the difference between the experimental flow inside the pipe and the unbounded flow assumed for the simulation. As mentioned above, stable vortex breakdowns are produced inside the pipe with a divergent wall or without. Although some differences might exist between the two configurations, we assume the essential ingredients remain for vortex breakdown in unbounded flow. Experimentally, vortex breakdown is easily observed in a pipe at moderate Reynolds number which makes quantitative measurements less difficult.

In its present form the vortex filament method does not explicitly include the effect of viscous diffusion. Therefore, we cannot say anything about the effect of Reynolds number on the breakdown process itself. We assume this process to be dominated by nonlinear inviscid effects. However, the upstream profiles within the vortex depend on Reynolds number as well as the vane angles which control the amount of swirling. However, by shaping the vortex filaments upstream of breakdown we can reproduce any desired velocity (and hence vorticity) profiles. In this sense we can follow changes in Reynolds number, and in the present simulation we attempt to simulate a vortex breakdown occurring at an experimental Re = 2300.

For numerical purposes, we divided the flow domain into four axial subregions (Fig. 9). For simplicity just one filament is shown. Regions I, II, and IV have predetermined filament geometries. Only in region III is the flow simulated fully. Regions I, II, and IV are constructed to provide high-quality boundary data for region III. Regions I and IV consist of straight, semi-infinite filaments that induce a swirl component on the filaments in region III. Here, analytical expressions were used for the induced velocity. For example, if one of these semi-infinite filaments, parallel to the x-axis, extends from (x_0, y_0, z_0) to minus infinity, the analytical induced velocity is as follows:

$$V_x = 0$$

$$V_y = -(\Gamma/4\pi)(z - z_0)F \Bigg\rbrace \tag{16}$$

$$V_z = (\Gamma/4\pi)(y - y_0)F$$

where

$$F = \{(x_0 - x)/[(x - x_0)^2 + (y - y_0)^2 + (z - z_0)^2 + A]^{1/2} + 1\}/[(y - y_0)^2 + (z - z_0)^2 + A]$$

$$A = \alpha(\sigma_i^2 + \sigma_j^2)/2$$

Region II consists of spiral or helical filaments which rotate and translate with fixed, predetermined velocities. The filaments in this region also induce velocity on the filaments in region III. Filament geometries and strengths in region II were determined as in the previous section. Thus the filaments in region III move according to an induced velocity from the filaments of region III as well as all other regions, using the dynamic equation, the Biot-Savart Law.

A Runge-Kutta fourth-order scheme was used for time-integration. Special attention was given to the filaments of region II. Because the Runge-Kutta scheme requires four different substeps to obtain the final solution at each time-step, we must use three different geometries other than the "exact geometry" to simulate precisely the Runge-Kutta errors that are being made in the upstream part of region III. Both the radius and phase angle were precalculated for each substep and stored in the program.

At each time-step node points were redistributed and, if necessary, added to each filament to maintain a nearly constant distance between points. This was accomplished by using a parametric spline fit to obtain the space curve defining a given filament.

At present we have insufficient knowledge about the initial disturbance necessary to produce vortex breakdown. Each type of vortex breakdown might need a different initial perturbation. At least it might be natural to consider that the three-dimensional type breakdown will need a three-dimensional disturbance. Preliminary axisymmetric calculations showed that a small amplitude disturbance on a vortex with no axial flow resulted only in weak traveling waves, but a large amplitude disturbance causes breakdown similar in appearance to wave-breaking. Experimentally, vortex breakdown is sometimes very sensitive to a disturbance in that a change in breakdown pattern occurs even if the same upstream conditions are maintained. In this report we present results for two initial disturbances. Case I had an axisymmetric disturbance and Case II had a three-dimensional disturbance.

The top function (t = 0) in Fig. 10a shows the initial geometry of the vortex filaments used for Case I and represents a large amplitude disturbance. The region of full simulation (region III) extends over the range $0 < x < 5$. In $0 < x < 3$, the helical geometry of the upstream flow was used, but in $3 < x < 4$, the helices gradually reverse pitch and the pitch was elongated by a factor of 1.4 in this decelerating region. In $4 < x < 5$, straight filaments were used.

Figure 10 also shows the time variation in the vortex filaments. The time-step was 0.2. A uniform axial velocity of 0.4 (potential flow) was added to that induced by the vortex filaments. This value was chosen after the results of preliminary runs were available, giving us an estimate of the speed of the disturbance. If this flow component is not chosen with some accuracy the disturbance will rapidly move toward one of the computational boundaries. However, this value does not play an essential part in flow pattern, because this is just the moving frame through which we see the phenomenon. Alternatively, one could continually adjust the free-stream component during the simulation to keep the disturbance centered. During the first few time-steps, a remarkable vortex swelling can be seen in the downstream region where the initial disturbance had a flow reversal (t = 1). This swelling moves downstream (t = 2). At later times these vortex filaments are elongated in the axial direction and in particular the filaments in the third ring appear almost parallel to the x-axis (t = 2 and t = 3). Just downstream of this region a narrow region with small pitch can be observed (t = 3). A central region which appears devoid of filaments due to the elongation and straightening of the filaments can also be seen at t = 6 in the middle of the picture. This region moves upstream and is a manifestation of the axisymmetric vortex breakdown. On the other hand, at t = 4 the filaments in the second and third rings show disorder just downstream of the center of the picture, followed by a contraction toward the x-axis near the downstream boundary. In contrast with this, the filaments in the outermost ring show slight expansion near the downstream boundary with some contraction upstream. At later times the outermost filaments establish a wavy pattern downstream of the first expansion. At t = 6 most filaments have become very disordered near the downstream boundary. Just upstream of this expansion the filaments of the second and third rings have become "untied" and elongated in the axial direction. Another interesting feature is that the filaments in the innermost ring contract to $r \simeq 0$ at the station where the outer filaments show the expansion at t = 2. This region of contraction has a long axial extent by t = 3 and then moves downstream with time.

In Case II we added a three-dimensional perturbation to the initial disturbance as shown in Fig. 10b (t = 0). The perturbation was caused by adding a radial displacement to each filament which was a sinusoidal function of theta (wavenumber = 1) and was nonzero and sinusoidal in x for $3 < x < 4$. It can be seen that differences in the filament configurations between Case I and Case II persist in time but remain confined to the downstream end of the computational domain.

Figure 11 shows the contours of axial velocity. Solid lines denote positive values and dashed lines negative values. Figure 11a shows Case I. Initially (t = 0), a downstream region of low axial velocity is shown as expected from the initial geometry of the filaments. By t = 1 this low-velocity region has gone through the downstream boundary and cannot be seen. Instead a high-velocity region appears. Between t = 1 and t = 2 this high-velocity region enlarges and moves downstream. At later times we see the development and enlargement of a low-velocity region upstream of the high-velocity region. Meanwhile, the peak velocity in the high-speed region is decreasing. At t = 7 and t = 8 we see another interesting feature. Near the downstream boundary another low-velocity region appears. Apparently, a second breakdown is occurring near the downstream boundary. Experimentally it is very often observed that axisymmetric vortex breakdown is followed by a second breakdown of the spiral type. In the experiment used to determine the upstream conditions a clear spiral-type vortex breakdown was observed. However, the axisymmetric initial disturbance for Case I only leads to axisymmetric flow.

Next, we discuss Case II (Fig. 11b), having a three-dimensional initial disturbance. Generally, Case II shows a pattern similar to that of Case I. However, we again see that three-dimensionality remains at later times, but only near the downstream boundary. As seen at $t = 5$ and later, the contours in the first breakdown are very similar to those in Case I and appear axisymmetric. But the second breakdown is distorted, not axisymmetric, and appears to be rotating around the x-axis (as seen in the downstream region at $t = 7$ and 8). This is suggestive of a vortex breakdown of the spiral type.

Figure 12 shows the theta velocity contours. For Case I at $t = 0$, the contours show no disturbance in the theta velocity because the filaments are distorted initially only in the theta direction. At $t = 1$, swelling of contour lines can be seen in the region of the initial perturbation. At $t = 2$ an interesting phenomenon appears downstream. Another swelling after the first swelling can be seen near the downstream boundary. At this time the swelling of the filaments near the x-axis seen at $t = 1$ has disappeared. The contours at $t = 3$ are similar to those at $t = 2$. Between $t = 2$ and $t = 4$ the axial position of the maximum swelling of the level 3 contour clearly moves upstream. After $t = 6$ the first swelling spreads to the contours near the x-axis. The first and the second swellings correspond to the two breakdowns observed above.

For Case II (Fig. 12b) we see that at $t = 0$ the contour lines have a slightly crooked pattern for $3 < x < 4$ where the initial three-dimensional disturbance was imposed. At $t = 1$ we can see the clear three-dimensional wavy pattern inside the region of swelling. At $t = 2$ the three-dimensionality moves toward the downstream boundary and seems to disappear until $t = 7$. At $t = 7$ and $t = 8$ we clearly observe three-dimensionality near the downstream boundary and a comparison of the contours at these two times indicates a rotating disturbance. This is in contrast with the first breakdown whose contours appear to be nearly axisymmetric and agree well with those of Case I. We conclude that the complete pattern of an axisymmetric vortex breakdown followed by a breakdown of the spiral type was simulated by allowing for three-dimensionality.

5. CONCLUDING REMARKS

The vortex-filament method was applied to the numerical simulation of vortex breakdown, which is intrinsic to the longitudinal vortex. Generally, there are three types of vortex breakdown: axisymmetric, spiral, and double helix. In this paper we simulated the axisymmetric type of vortex breakdown. Generally, it is difficult to obtain information experimentally due to the sensitivity of breakdown to any perturbation. Calculated results should be helpful to understand this complicated phenomenon. The principal vortex region was represented by the multiple filaments. One filament is not enough to represent this complicated flow field. In particular, the present method can include axial flow which is often observed in physical vortices.

Vortex breakdown was simulated under the assumption of nonlinear, inviscid dynamics of vorticity using the three-dimensional vortex-filament method. Viscous effects are assumed to be important only in forming upstream velocity profiles. Upstream profiles were simulated accurately with helical vortex filaments by choosing pitch and circulation to minimize the error. First, an accuracy check was performed for a cylindrical flow with simple analytical functions for the axial and theta velocities. This profile was the idealization for the experimental data used for the vortex-breakdown simulation. Comparison of the simulated results with the idealized flow suggests that the flow field can be simulated to any accuracy by increasing the number of the filaments.

Two cases, Case I and Case II, were calculated to simulate axisymmetric-type breakdown. In order to create a strong initial disturbance, the filaments in the downstream axial region were provided with a change in pitch. We used two kinds of initial disturbance to see their effect on vortex breakdown. Case I had an axisymmetric disturbance and Case II had a three-dimensional disturbance. Filament configurations and contour plots of velocity showed, for both cases, two simultaneous vortex breakdowns. One vortex breakdown was similar in both cases and was axisymmetric. The other vortex breakdown was axisymmetric for axisymmetric disturbances and three dimensional for three-dimensional disturbances. The latter case agrees with the experimental observations where an axisymmetric vortex breakdown is followed by a spiral-type breakdown.

Other types of breakdown (spiral and double-helix) should be possible to simulate by this method. The present method can also be applied to other vortex flows with axial velocity profile.

REFERENCES

1. Peckham, D. H. and Atkinson, S. A., "Preliminary Results of Low Speed Wind Tunnel Tests on a Gothic Wing of Aspect Ratio 1.0," Aeronautical Research Council C.P. No. 508, 1960.

2. Sarpkaya, T., "On Stationary and Travelling Vortex Breakdown," J. Fluid Mech., Vol. 45, 1971, pp. 545-559.

3. Lambourne, N. C. and Bryer, D. W., "The Bursting of Leading Edge Vortices — Some Observations and Discussion of the Phenomenon," Aeronautical Research Council R and M 3282, 1962.

4. Hall, M. G., "Vortex Breakdown," Annual Review of Fluid Mechanics, Vol. 4, 1972, pp. 195-218.

5. Faler, J. H. and Leibovich, S., "Disrupted States of Vortex Flow and Vortex Breakdown," Phys. Fluids, Vol. 20, 1977, pp. 1385-1400.

6. Faler, J. H. and Leibovich, S., "An Experimental Map of the Internal Structure of a Vortex Breakdown," J. Fluid Mech., Vol. 86, 1978, pp. 313-335.

7. Escudier, M. P. and Zehnder, N., "Vortex-Flow Regimes," J. Fluid Mech., Vol. 115, 1982, pp. 105-121.

8. Leibovich, S., "The Structure of Vortex Breakdown," Annual Review of Fluid Mechanics, Vol. 10, 1978, pp. 221-246.

9. Benjamin, T. B., "Theory of the Vortex Breakdown Phenomenon," J. Fluid Mech., Vol. 14, 1962, pp. 593-629.

10. Ludwieg, H., "Zur Erklärung der Instabilität der über Angestellten Deltaflügeln Auftretenden Freien Wirbelkerne," Z. Flugwiss., Vol. 10, 1962, pp. 242-249.

11. Hall, M. G., "A Numerical Method for Solving the Equations for a Vortex Core," Aeronautical Research Council R and M 3467, 1965.

12. Grabowski, W. J. and Berger, S. A., "Solutions of the Navier-Stokes Equations for Vortex Breakdown," J. Fluid Mech., 1976, pp. 525-544.

13. Leonard, A., "Vortex Methods for Flow Simulation," J. Comp. Phys., Vol. 37, 1980, pp. 289-335.

14. Del Prete, V., "Numerical Simulation of Vortex Breakdown," Lawrence Berkeley Laboratory Report 8503, Berkeley, Calif., 1978.

15. Oshima, Y. and Asaka, S., "Interaction of Multi-Vortex Rings," J. Phys. Soc. Japan, Vol. 42, 1977, pp. 1391-1395.

16. Nakamura, Y., Leonard, A., and Spalart, P. R., "Vortex Simulation of an Inviscid Shear Layer," AIAA Paper 82-0948, 1982.
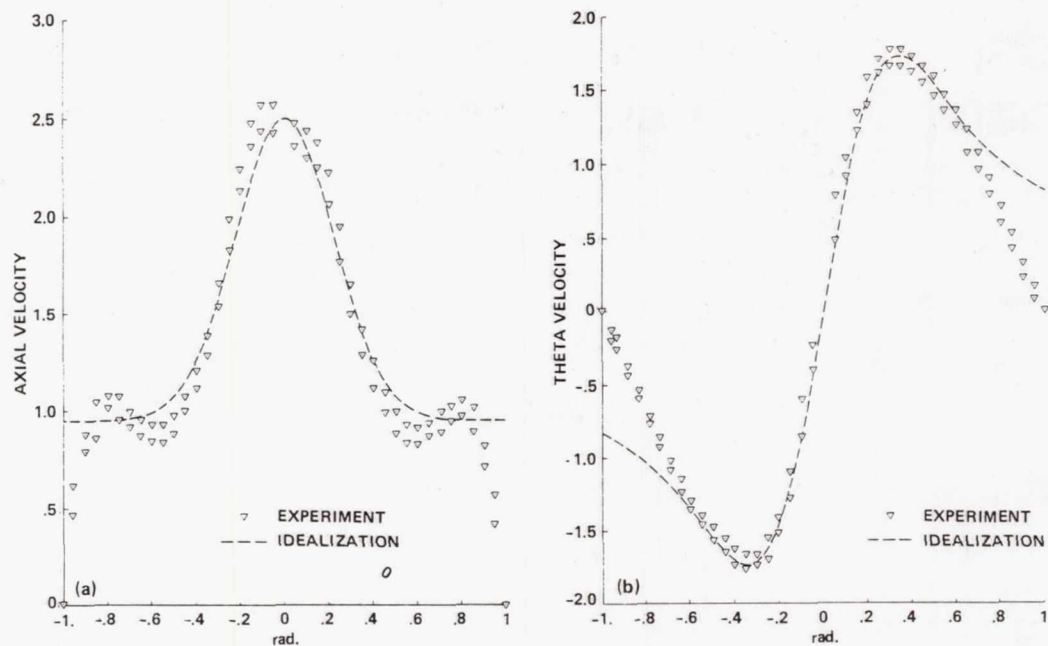
Fig. 1. Velocity profiles in the upstream region. (a) Axial velocity; (b) Theta velocity.
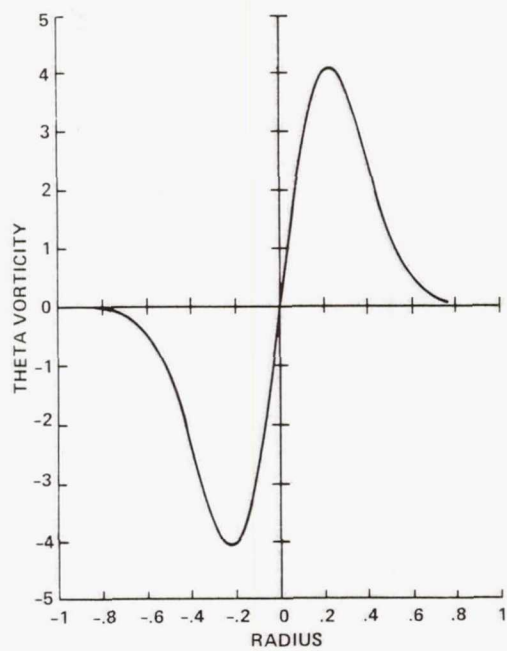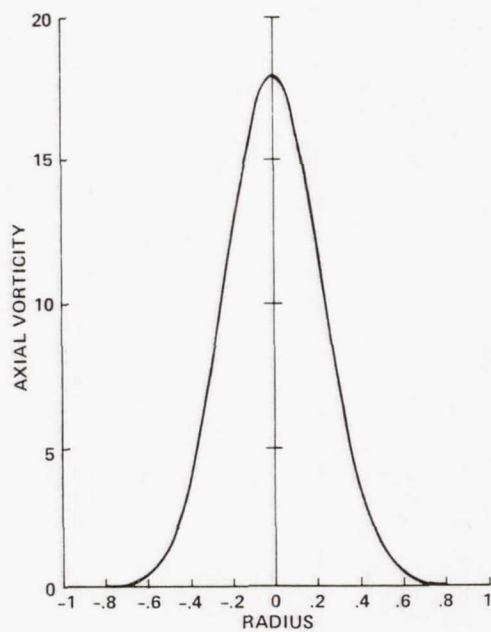

Fig. 2. Upstream theta vorticity.

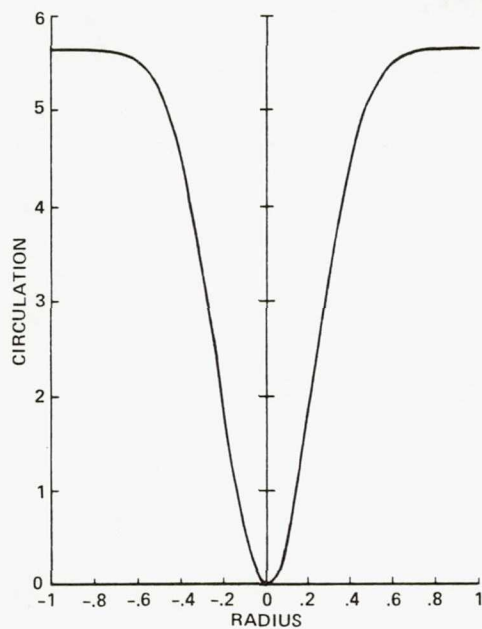Fig. 3. Upstream axial vorticity.
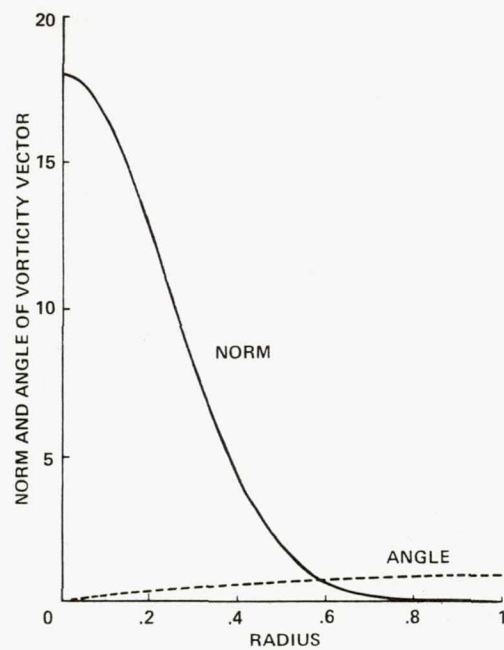
Fig. 4. Circulation.

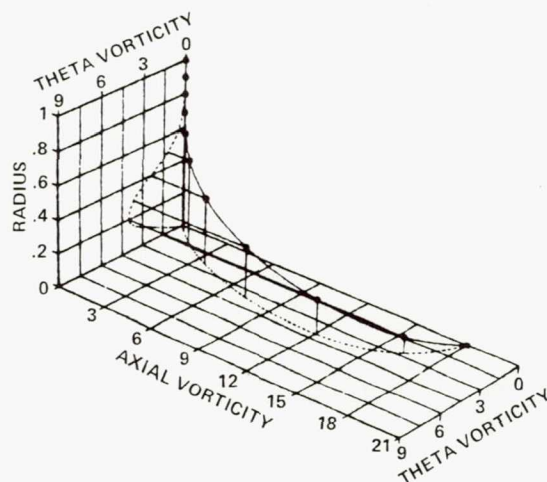Fig. 5. Norm and angle of the vorticity vector of the idealization as a function of radius.

Fig. 6. Three-dimensional view of the vorticity-vector distribution.
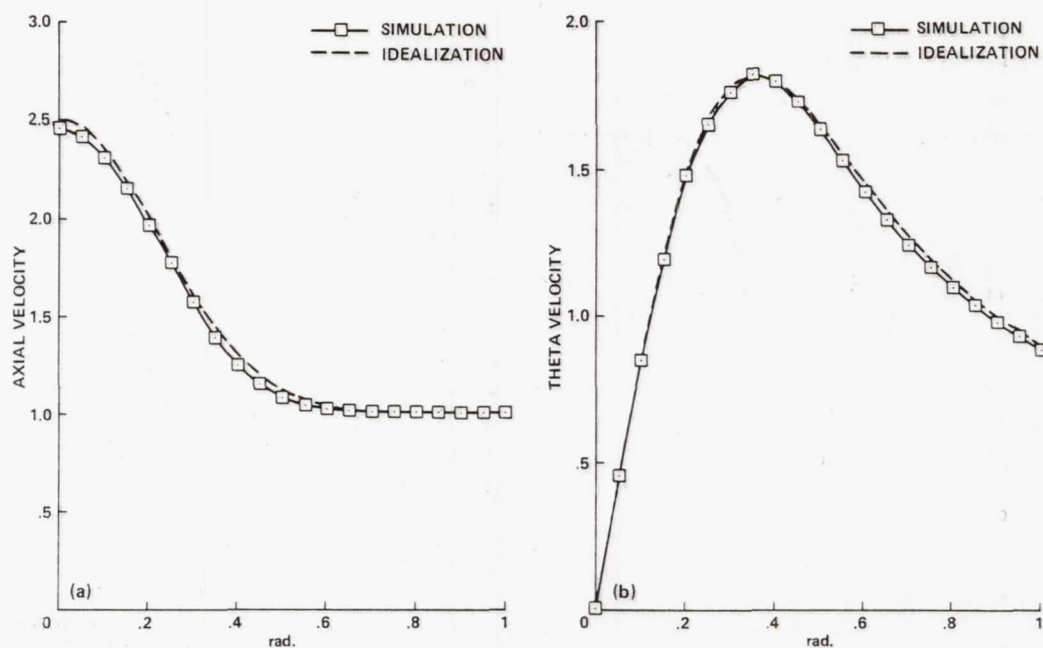
Fig. 7. Comparison between the calculated velocity distribution along the z-axis and the idealization. (a) Axial velocity; (b) Theta velocity.
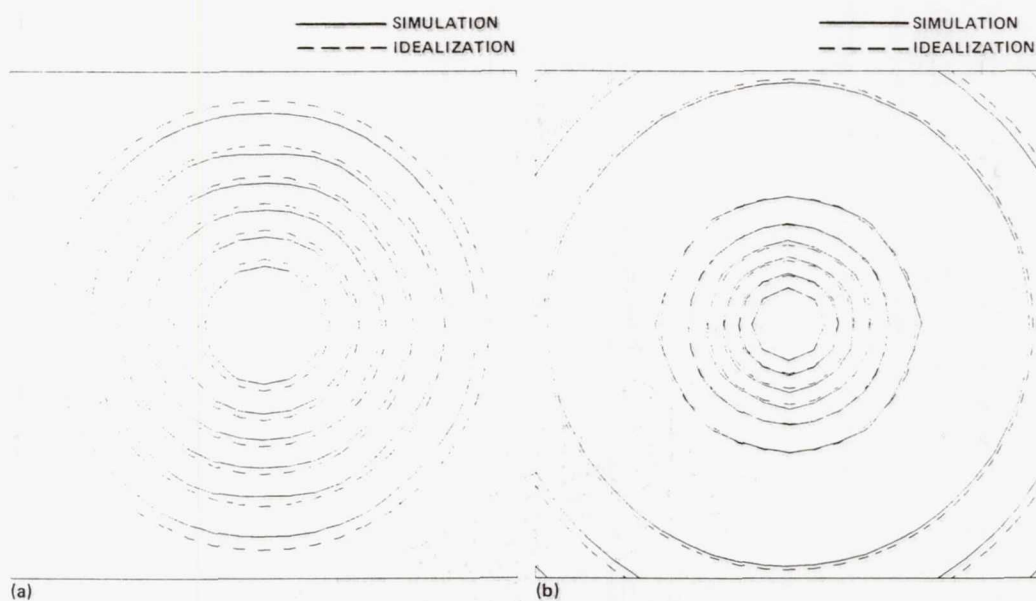
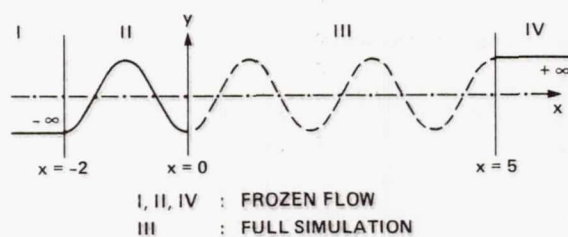Fig. 8. Upstream velocity contours in a cross section. (a) Axial velocity; (b) theta velocity.

I, II, IV : FROZEN FLOW
III : FULL SIMULATION

Fig. 9. Computational regions for filament to calculate induced velocity.

10
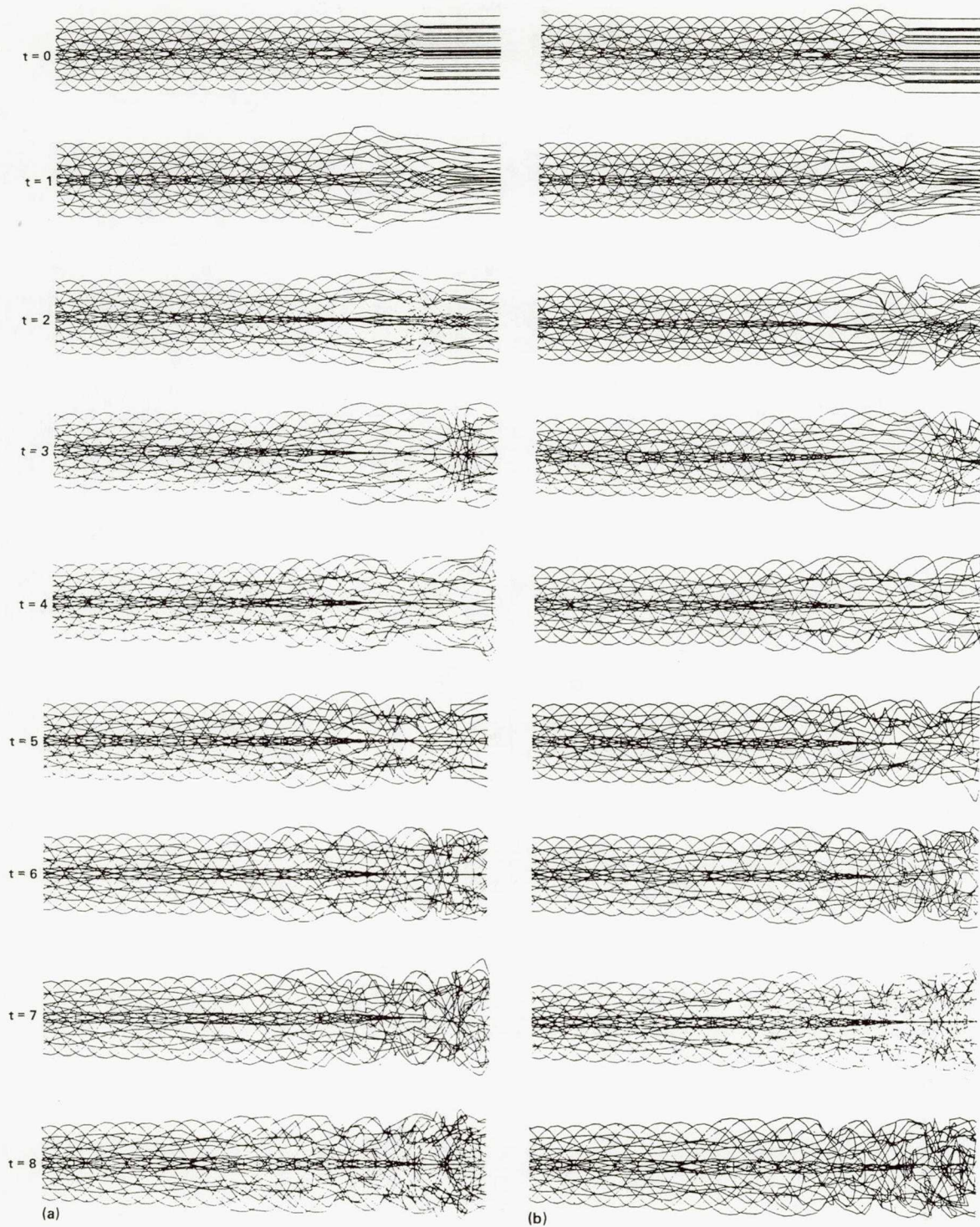
Fig. 10. Evolution of vortex filaments. (a) Case I; (b) Case II.

11

MIN = –0.4374 MAX = 1.890   MIN = –0.4285 MAX = 1.890

t = 0

MIN = 0.3267 MAX = 1.863   MIN = 0.3061 MAX = 1.863

t = 1

MIN = 0.3447 MAX = 1.859   MIN = 0.3649 MAX = 1.859

t = 2

MIN = 0.3951 MAX = 1.856   MIN = 0.3614 MAX = 1.856

t = 3

MIN = 0.4125 MAX = 1.855   MIN = 0.3437 MAX = 1.854

t = 4

MIN = 0.4454 MAX = 1.853   MIN = 0.4244 MAX = 1.853

t = 5

MIN = 0.3464 MAX = 1.851   MIN = 0.3569 MAX = 1.851

t = 6

MIN = 0.2254 MAX = 1.849   MIN = 0.1333 MAX = 1.849

t = 7

MIN = –0.02197 MAX = 1.846   MIN = –0.01307 MAX = 1.847

t = 8

(a)   (b)
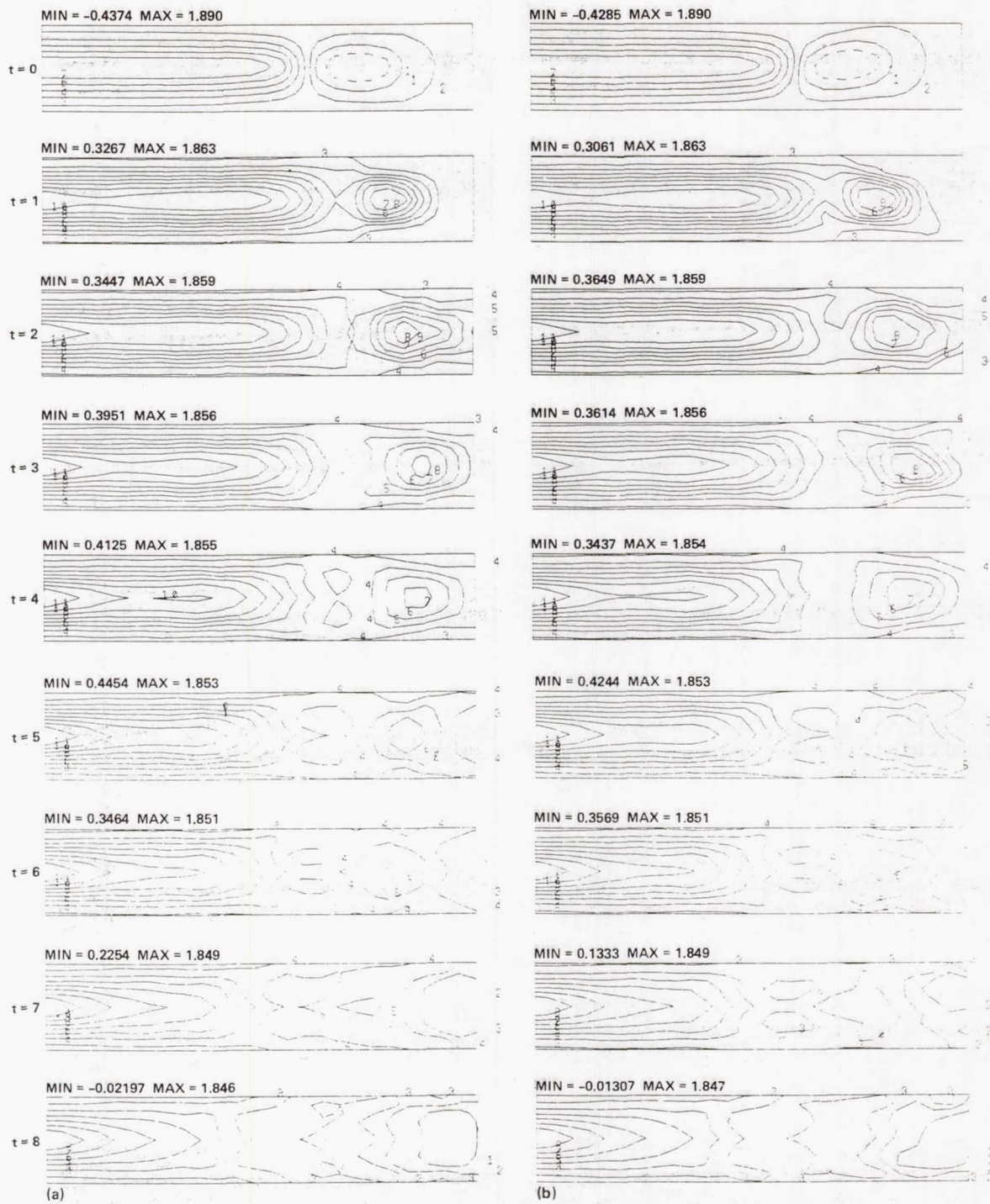
Fig. 11. Axial velocity contours. (a) Case I; (b) Case II.

MIN = -1.737 MAX = 1.737

MIN = -1.755 MAX = 1.761

t = 0

MIN = -1.734 MAX = 1.734

MIN = -1.729 MAX = 1.737

t = 1

MIN = -1.730 MAX = 1.730

MIN = -1.731 MAX = 1.730

t = 2

MIN = -1.728 MAX = 1.728

MIN = -1.728 MAX = 1.728

t = 3

MIN = -1.712 MAX = 1.712

MIN = -1.712 MAX = 1.711

t = 4

MIN = -1.707 MAX = 1.707

MIN = -1.708 MAX = 1.706

t = 5

MIN = -1.717 MAX = 1.717

MIN = -1.717 MAX = 1.716

t = 6

MIN = -1.730 MAX = 1.730

MIN = -1.730 MAX = 1.729

t = 7

MIN = -1.725 MAX = 1.725

MIN = -1.725 MAX = 1.724

t = 8

(a)

(b)

Fig. 12. Theta velocity contours. (a) Case I; (b) Case II.

13

1. Report No. NASA TM-84334	2. Government Accession No.	3. Recipient's Catalog No.

4. Title and Subtitle	5. Report Date
NUMERICAL SIMULATION OF VORTEX BREAKDOWN BY THE VORTEX-FILAMENT METHOD	July 1983
	6. Performing Organization Code

7. Author(s)	8. Performing Organization Report No.
Y. Nakamura, A. Leonard, and P. R. Spalart	A-9263
	10. Work Unit No.
9. Performing Organization Name and Address	T-6470
NASA Ames Research Center Moffett Field, Calif. 94035	11. Contract or Grant No.
	13. Type of Report and Period Covered
12. Sponsoring Agency Name and Address	Technical Memorandum
National Aeronautics and Space Administration Washington, D.C. 20546	14. Sponsoring Agency Code 505-31-21-00-21

15. Supplementary Notes
Presented at AGARD Symposium on Aerodynamics of Vortical Type Flows in Three Dimensions. Point of Contact: A. Leonard, Ames Research Center, M/S 202A-1, Moffett Field, CA 95043 (415)965-6459 or FTS 448-6459

16. Abstract

The vortex-filament method was applied to the simulation of vortex breakdown. The principal vortex region was represented by multiple fila-ments, and an axial velocity component was induced by a spiral winding of the filaments. First, an accuracy check was performed for a cylindrical swirling flow with simple analytical expressions for the axial and theta velocities. The result suggests that the flow field can be simulated to any accuracy by increasing the number of filaments. Second, an axisymmetric-type vortex breakdown was simulated, with experimental data serving as upstream conditions. The calculated axial- and theta-velocity contours show the breakdown of the vortex, including a rapid change in the vortex core, followed axially by a recovery zone and then a second breakdown. When three-dimensional initial data are used the second breakdown appears to be of the spiral type in correspondence with experimental observations. The present method can easily be used to simulate other types of vortex breakdown or other vortex flows with axial velocity.

17. Key Words (Suggested by Author(s))	18. Distribution Statement
Numerical simulation Vortices Vortex breakdown	Unlimited Subject Category - 34

19. Security Classif. (of this report) Unclassified	20. Security Classif. (of this page) Unclassified	21. No. of Pages 16	22. Price* A02

*For sale by the National Technical Information Service, Springfield, Virginia 22161